Arch. Metall. Mater. **68** (2023), 1, 387-393

DOI: https://doi.org/10.24425/amm.2023.143673

NANFU ZONG[1*], ZHENG WANG[1], YANG LIU[2], XINGHONG LIANG[1], TAO JING[1]

COLUMNAR DENDRITE MORPHOLOGY AND SOLUTE CONCENTRATION OF GH3039 NICKEL-BASED SUPERALLOYS DURING WIRE AND LASER ADDITIVE MANUFACTURING: INSIGHTS FROM PHASE FIELD SIMULATIONS

Wire and laser additive manufacturing (WLAM) can produce outstanding mechanical properties of GH3039 nickel-based superalloys. A quantitative rapid phase field model with solute trapping kinetics has been developed during the rapid solidification process, where a range of process conditions are considered in terms of thermal gradients and pulling speeds. Intergranular hot cracking is found to occur at boundaries of tilted columnar dendrite in the GH3039 nickel-based superalloys. The simulations demonstrate that the phase field model considering the interface deflection can represent the dendrite growth during additive manufacturing more realistically. With the aid of numerical simulations, it is determined that dendrite growth morphologies transform from symmetrical columnar dendrite to tilted columnar dendrite as the interface crystallographic deflection is increased, while increasing the deflection angle can lead to uneven composition of material matrix, especially at the columnar dendrite interface. Solute concentrations at the columnar dendrite interface tend to promote hot cracking in additively manufactured Ni-based superalloy.

Keywords: Wire and laser additive manufacturing; phase field simulation; solute concentration; interface crystallographic deflection; columnar dendrite

1. Introduction

GH3039 nickel-based superalloys are mainly composed of Ni-Cr elements, and have lots of specific advantages, such as excellent high strength, oxidation resistance, weldability and high creep resistance, which can be applied to manufacture components on turbine engine combustor at elevated temperature [1]. The continuous casting technology is an effective method to manufacture metallic alloys and is widely used in the fabrication of alloy sheets [2-5]. Numerical simulations method has been widely used to analyze and optimize the casting process to improve the quality of products [6-9]. However, there are still challenge to fabricate parts with a high flexible design and tailored microstructures.

Wire and laser additive manufacturing (WLAM) [10] and selective laser melting (SLM) [11], also known as three-dimensional (3D) printing, are emerging manufacturing technologies. In comparison to casting, fine-grained structures have usually been achieved by additive manufacturing (AM) of metallic alloys due to the rapid solidification, which are conductive to produce outstanding mechanical properties in nickel-based superalloys layer by layer. Nonetheless, there has been a considerable variation in quality of manufactured materials [12].

During this wire and laser additive manufacturing process, the nickel-based superalloys studied in the present work solidified under extremely high thermal gradients and pulling speeds, exhibit a complex array of fine dendrites where solute concentration of alloying elements occurs [13]. In actuality, the solute concentration and dendrite arm spacing are two key points of columnar dendrites growth during the laser additive manufacturing process. The distribution and morphology of columnar dendrites in the molten pool needs to be predicted dynamically during the fast solidification process, the phase field (PF) numerical simulations make it possible to investigate evolution of solidification in the molten pool, which have attracted growing attention in the field of WLAM simulation [14-16]. Wang et al. [14-15] adopted the quantitative PF model to simulate the solidification parameters under different AM conditions, which indicate the G, R and G/R are related with the location of molten pool and AM conditions. Zheng et al. [16] formulated the time-

[1] TSINGHUA UNIVERSITY, MINISTRY OF EDUCATION, SCHOOL OF MATERIALS SCIENCE AND ENGINEERING, KEY LABORATORY FOR ADVANCED MATERIALS PROCESSING TECHNOLOGY, BEIJING 100084, CHINA
[2] JIANGSU CHANGQIANG IRON AND STEEL CORP., LTD., JIANGSU 214500, CHINA
* Corresponding author: zongnan512712_2005@163.com

dependent equations for G and R in the molten pool. Coupled with the transient conditions, the solidification evolution in the molten pool was simulated by the quantitative PF model.

The previous researches [14-15] demonstrate the ability and accuracy of the quantitative PF model simulating solidification evolution in WLAM. However, researches ignored the angle between the crystallographic orientation and the z-axis (vertical). Based on the above studies, the potential influence of crystallographic orientation on manufactured materials proves to be a factor that needs to be considered in order to gain reliable information about columnar dendrite and solute concentration. In the present study, the quantitative PF model considering the crystallographic orientation has been developed to reveal solidification behavior in the molten pool more realistically, especially at the late stage of solidification in welding. The investigations can provide theoretical basis for optimization of additive manufacturing parameters by the control of columnar dendrite and solute concentration.

2. Phase-field simulation and dendrite morphology of additive manufacturing

2.1. Phase-field model for GH3039 alloy solidification

The transient condition macroscopic model is applied to obtain the time-dependent pulling speed Vp and thermal gradient G by Zheng [13,16]. The macrograph of molten pool is shown in Fig. 1. It is composed of two half ellipsoids. The rear ellipsoid is the solidification area of the molten pool. The yellow region showed in Fig. 1 is the computational domain. The depth and rear length of the solidification area are defined as al and bl respectively.

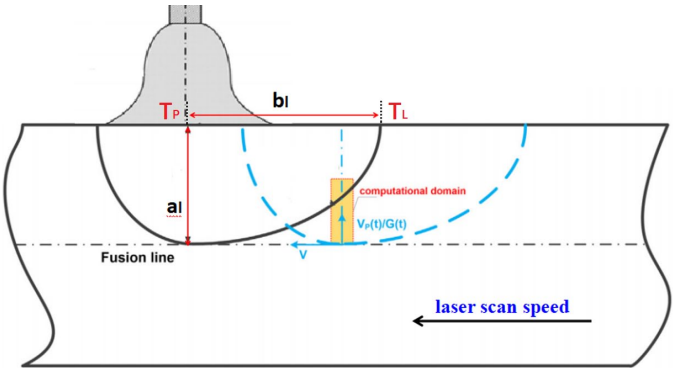

Fig. 1. The shape and motion of molten pool at early stage

The temperature at molten pool edge is the equilibrium liquidus temperature. *Tp* is the temperature value at the center of molten pool, which is maximum value of temperature in the molten pool. *V* is the laser scan speed (the moving velocity of molten pool). $Vp(t)$ and $G(t)$ are the time-dependent pulling velocity and temperature gradient, respectively. Hence, $Vp(t)$ and $G(t)$) can be expressed as:

$$V_P(t) = \frac{a_l V^2 t}{\sqrt{V^2 t^2 \left(a_l^2 - b_l^2\right) + b_l^4}} \tag{1}$$

$$G(t) = \frac{T_P - T_l}{\sqrt{V^2 t^2 + a_l^2 \dfrac{1 - V^2 t^2}{b_l^2}}} \tag{2}$$

Dendrite growth dynamics can be investigated by a powerful tool of phase-field approach, which can make up for lack of experimental studies on dendrite growth during additive manufacturing. The calculation details of the phase-field model can be found in elsewhere [14-16]. Specifically, we modified the phase-field model to simulate the dendrite growth in the molten pool, considering the crystallographic deflection of S/L interface.

For cubic GH3039 alloys, a four-fold anisotropy function can be adopted:

$$a_s(\bar{n}) \equiv a_s(\theta_i + \theta_i^0) = 1 + \gamma_4 \cos 4(\theta_i + \theta_i^0) \tag{3}$$

where γ_4 is the anisotropy strength, θ_i is the angle between the normal direction of S/L interface and the temperature gradient direction, θ_i^0 is angle between the crystallographic orientation and the z-axis.

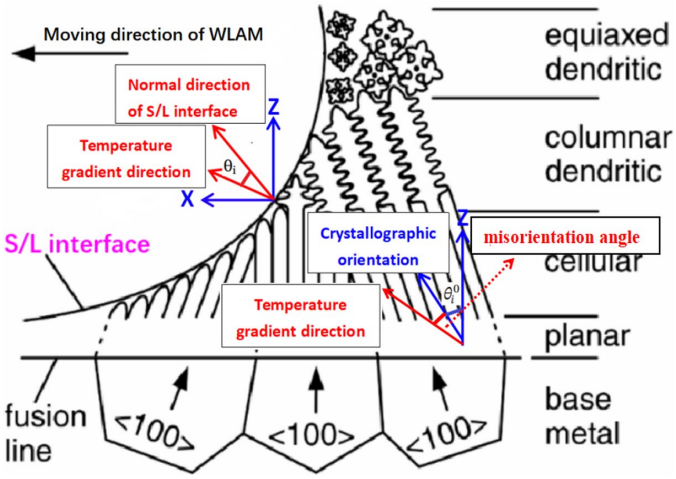

Fig. 2. The crystallographic deflection of S/L interface

Fig. 2 illustrates the crystallographic deflection of S/L interface, which can represent the solidification in the laser melt pool during WLAM accurately, especially at the late stage of solidification. For this quantitative interface phase-field model, the coupling parameters and thermophysical parameters of GH3039 alloy have been taken from our previous references [15]. The growth conditions are complex due to their variable thermal histories. Therefore, understanding of melt pool solidification behavior is essential under transient conditions.

2.2. Characterization of microstructure evolution

The GH3039 super alloy wire was employed as the original material. The chemical compositions of the metal wire are shown in TABLE 1. The substrate material was 45# steel sheets and the substrate surface was grounded before laser fusion. Chemical composition of CH3039 super alloy wire is presented in TABLE 1.

TABLE 2 lists the main characteristics of the laser processing parameters in this study, the time-dependent solidification parameters of the phase-field model can be determined according to the above parameters.

TABLE 1

Chemical composition of CH3039 super alloy wire

Element	C	Cr	Mo	Al	Ti	Si	Fe	Nb	Ni
Wt%	0.38	19.04	1.86	0.60	0.48	0.19	1.38	0.77	Bal.

TABLE 2

Laser processing parameters

Parameter	Value
Laser power, P (KW)	2
Equivalent laser scan speed, V (mm/s)	4.0
Depth of the laser melt pool, h (mm)	1.8
Width of the laser melt pool, b (mm)	2.6

Finally, the characteristic parameters of molten pool during wire and laser additive manufacturing can be obtained by the finite element method. Due to the high laser speed, we chose the Goldak double ellipsoid heat source to reflect the thermal transport property of the wire and laser additive manufacturing.

Fig. 3 shows the typical grain distribution and morphologies of the longitudinal section for the cladding layers of the GH3039 super alloy. As shown in Fig. 3, there are two typical columnar dendrite morphologies. A cluster of columnar dendrites are mainly distributed at the bottom of the cladding layers, one typical columnar dendrites are nearly vertical to the surface of substrate, the other typical columnar dendrites have the angle between the normal direction of substrate surface. The columnar dendrites were almost distributed at the bottom of the substrate and then they grow along their preferred crystalline orientations in the shape of columnar dendrites during the wire and laser additive manufacturing (WLAM). The epitaxial growth of columnar dendrites with different orientations has a profound influence on the final microstructure as well as segregation patterns, which determine several properties of metallic materials from the laser melt pool bottom to its top. There are two characteristic directions, thermal gradient direction and the preferred crystalline orientation, the angle between the two directions is usually defined as the misorientation angle.

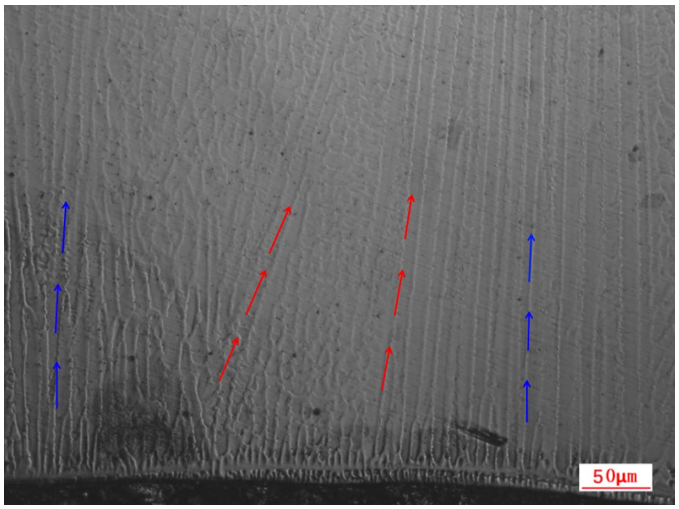

Fig. 3. OM images showing the dendrite growth direction and morphologies of the longitudinal section

3. Results and discussion

3.1. Evolution of dendrite morphology during transient conditions

Understanding the evolution of columnar dendrite and interface velocity is critical for analysis of segregation of the solute and spacing evolution. In fact, the growth competition between columnar dendrite and degenerate seaweed can be much more complex. The evolution of columnar dendrite of GH 3039 alloy has been simulated with laser power of 2 KW and laser scan speed of 4 mm/s under transient conditions. The interface morphologies transform into a relatively uniform cellular dendrites array through the stages of planar interface, rudiment of cells and cellular submerging stage. Due to the accumulation of solute, the planar instability occurs, which reflects the planar crystal transform to the cellular crystals, as shown in Fig. 4(a), (b) and (c). Comparing with morphological evolution without interface crystallographic deflection, the morphological evolution of dendrite growth with the S/L interface deflection, can reproduce solidification process in the molten pool more accurately. Morphological evolution of dendrite growth in transient conditions with interface crystallographic deflection of 45° are shown in Fig. 5. It can be seen that the dendrite growth morphologies transform from symmetrical columnar dendrite (Fig. 4) to tilted columnar dendrite (Fig. 4) as the interface crystallographic deflection is increased.

At the early stage, the tip velocity of dendrite growth is faster than that without interface crystallographic deflection. It can be seen that the dendrite growth morphologies transform from symmetrical columnar dendrite to tilted columnar dendrite as the interface crystallographic deflection is increased.

Fig. 6 represents the dendrite tip velocity along the dendrite growth direction as a function of time. Comparing with the maximum velocity without interface crystallographic deflection, the maximum velocity with interface crystallographic deflection of 45° is faster and it arises at later time in the present study.

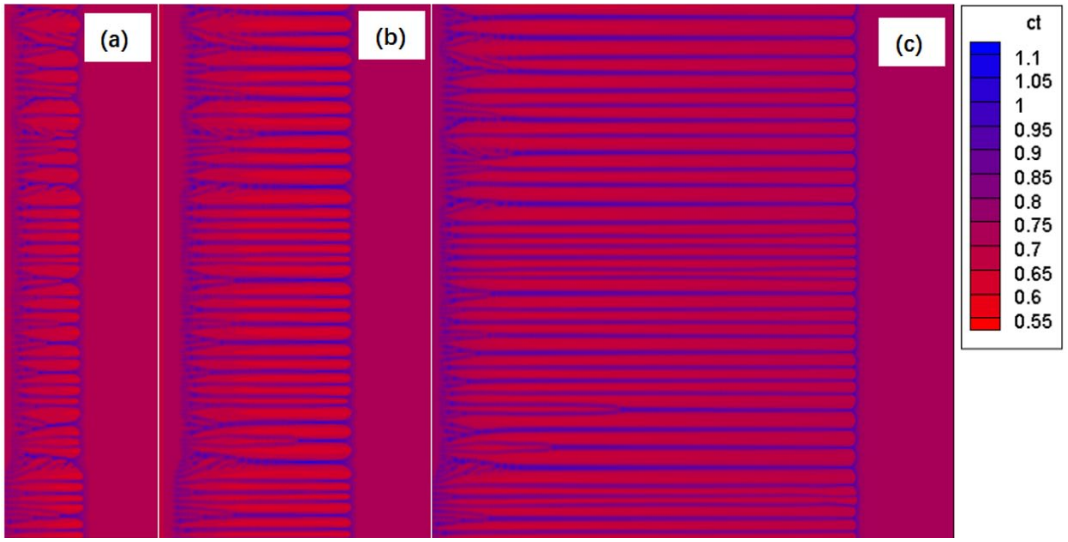

Fig. 4. Morphological evolution of dendrite growth in transient conditions without interface crystallographic deflection (a-c). Growth time: (a) 0.20 s, (b) 0.24 s, (c) 0.38 s

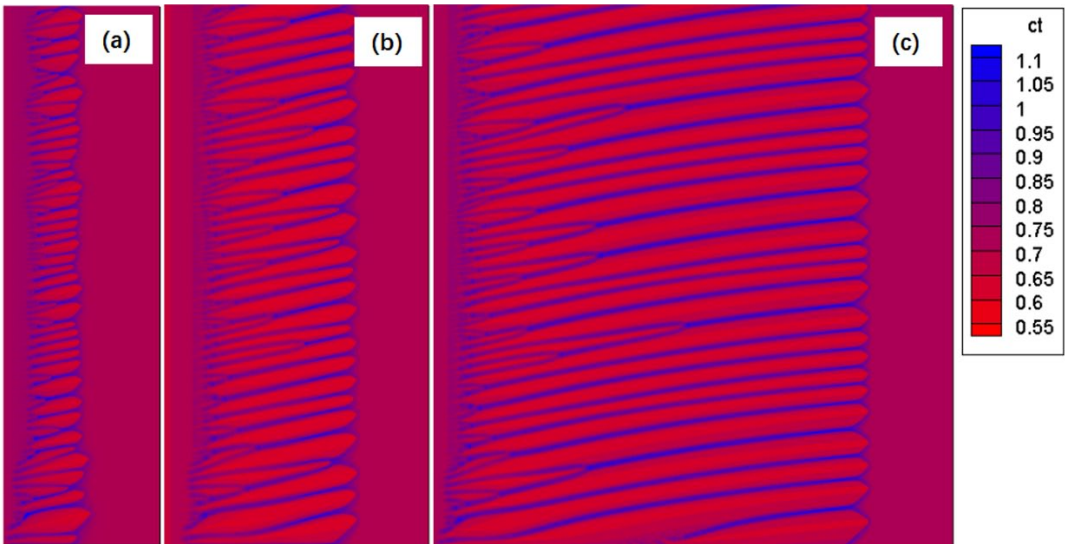

Fig. 5. Morphological evolution of dendrite growth in transient conditions with interface crystallographic deflection of 45° (a-c). Growth time: (a) 0.20 s, (b) 0.24 s, (c) 0.38 s

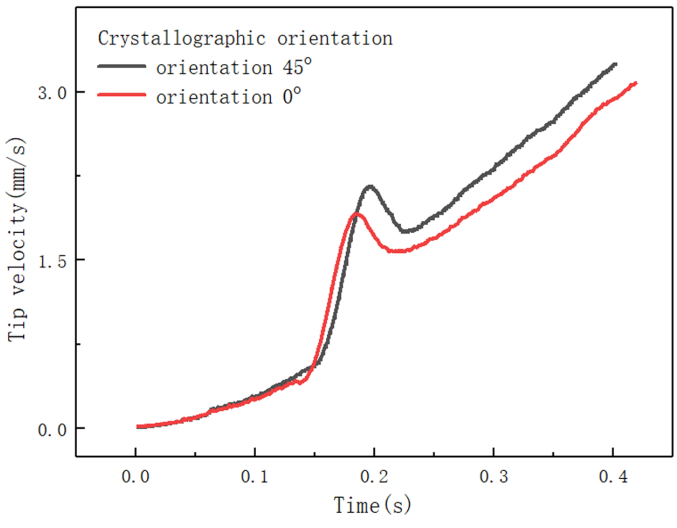

Fig. 6. The dendrite tip velocity as a function of time

3.2. Solute concentration and solidification cracking

Understanding the evolution of columnar dendrite and solute concentration is critical for analysis of solidification cracking. Fig. 7 shows the evolution of solute concentration during transient conditions with crystallographic orientation 0°and crystallographic orientation 45°. X-axis of Fig. 7 illustrates the growth direction of columnar dendrite, Y-axis of Fig. 7 illustrates the distance along the longitudinal section of samples.

Fig. 8 shows the comparisons of the lines of solute concentration under different crystallographic orientation. The purple dashed lines are represented the upper and lower limits of the solute concentration boundary, and the calculated area is located at the melt pool bottom. The upper limit of solute concentration with crystallographic orientation 45° is larger than that without

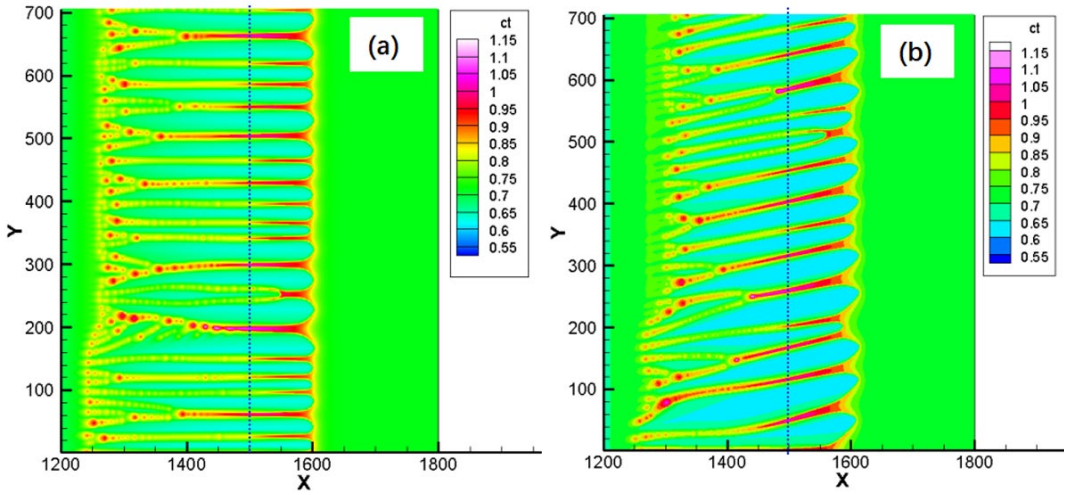

Fig. 7. The evolution of solute concentration during transient conditions: (a) with crystallographic orientation 0°, (b) with crystallographic orientation 45°

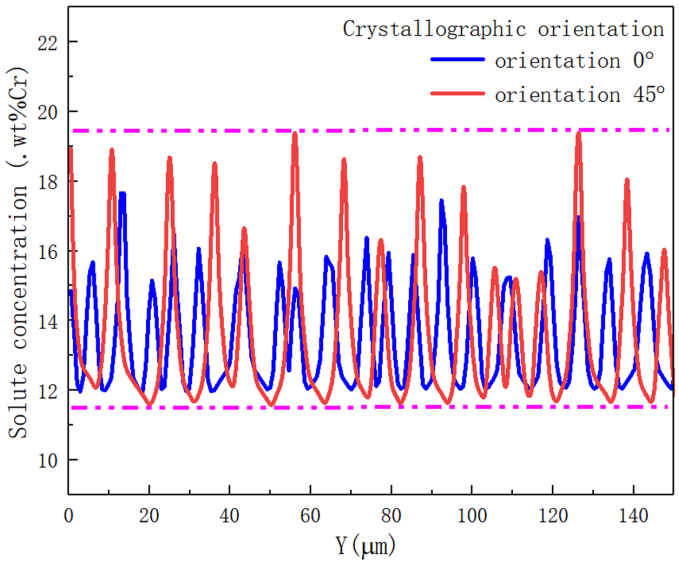

Fig. 8. Lines of solute concentration under different crystallographic orientation

crystallographic orientation, however, the lower limit of solute concentration with crystallographic orientation 45° is smaller than that without crystallographic orientation. Moreover, increasing the deflection angle can lead to uneven composition of material matrix, especially at the columnar dendrite interface.

In order to confirm the elemental composition of dendritic solute segregation, EDX line scan analyses were implemented at various grain structures. As shown in Fig. 9(a), the morphology of columnar dendrite was nearly vertical to the surface of substrate. As shown in Fig. 9(b), the tilted columnar dendrite has a deflection angle to the normal direction of substrate surface. The EDX results of relative counts along the longitudinal section of samples were shown in Fig. 9(c), which can confirm the analysis results of solute concentration under different crystallographic orientation. The absence of Cr signal indicates the high chromium content in the samples, the crystallographic orientation can increase the fluctuation of Cr element content.

The Cr concentration variations are studied in the inter cellular regions, the center of the columnar dendrite tips and deep into the columnar dendrites. The predicted Cr concentration from the PF simulations agrees well with the EDX results of experiment. A detailed analysis of EDS line scan indicated the relative contents (w%) for Cr varied from 10.8% to 20.1%, at different positions of the line scan (Fig. 9). Fig. 8 has shown the Cr contents (w%) varied from 11.2% to 19.5% by PF model. The Cr solute is easy to diffuse to columnar dendrite side when the columnar dendrite has a deflection angle to the laser scan speed. At that circumstance, there will be a solute concentration peak at columnar dendrite side, which makes the constitutional undercooling is higher at columnar dendrite side. This phenomenon promotes cellular dendritic growth.

Cracking was observed to be mostly intergranular as shown in Fig. 10. The initial crack can propagate through the material along the boundaries of of tilted columnar dendrites. Apart from dendrite boundaries, Cr solute concentrations were observed along coherent dendrite boundaries associated with sustained cracking. Thus further increasing the interface crystallographic deflection, dendrite growth morphologies transform from symmetrical columnar dendrite to tilted columnar dendrite, which accelerates crack initiation. Moreover, the solute concentration has the tendency to aggregate at the boundaries of columnar dendrite, the solute concentration leads to the weakening of the neighbouring dendritic network. Micro-segregation has the tendency to promote dendritic separate that can potentially mitigate crack initiation and propagation of the melt pool solidification due to external loading such as residual stress.

4. Conclusion

In this work, a quantitative rapid phase field model considering the interface deflection has been developed to simulate the dendrite growth in the molten pool during wire and laser additive manufacturing of GH3039 alloy. Evolution of dendrite

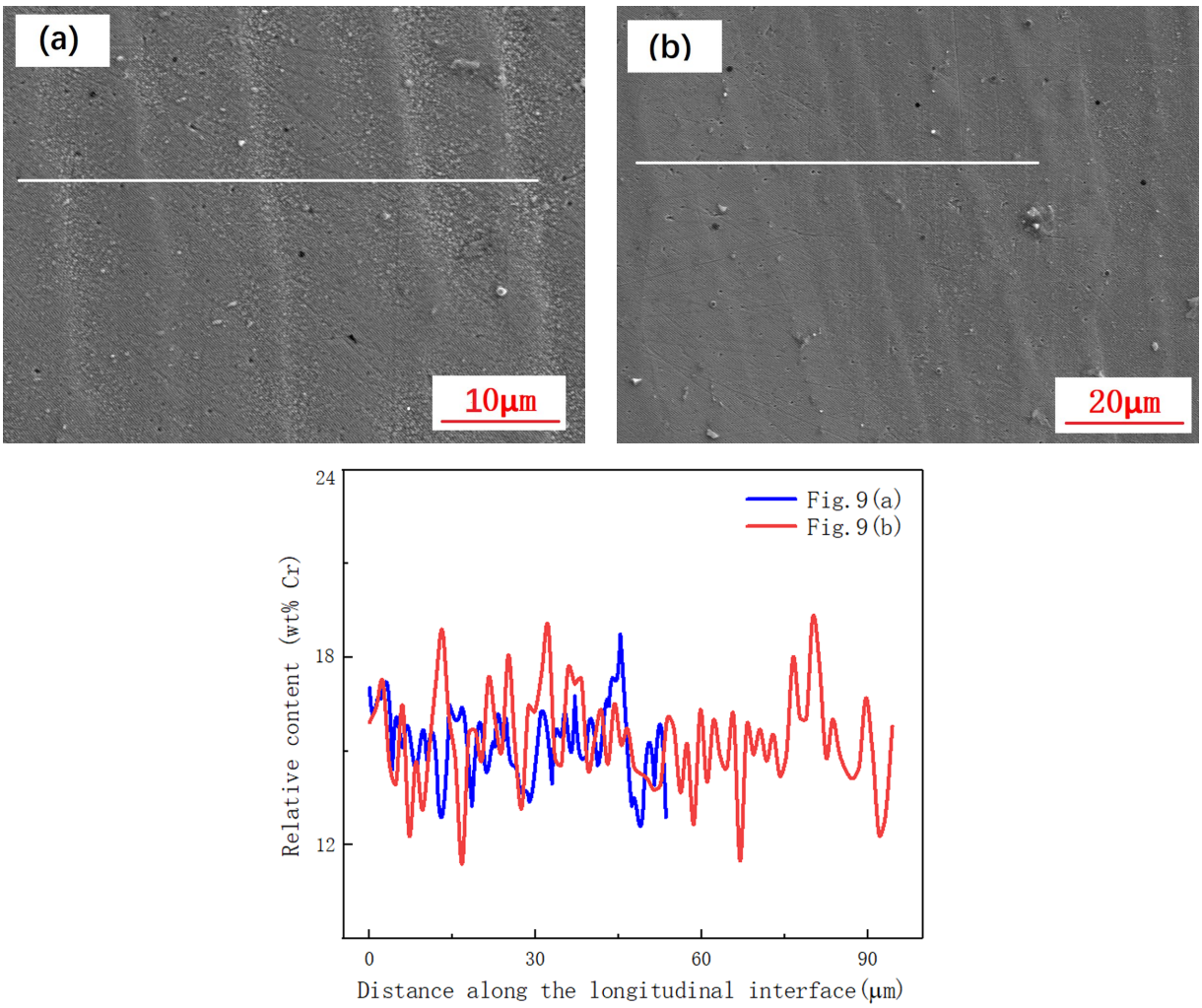

Fig. 9. EDX line scan analyses along the longitudinal section of samples

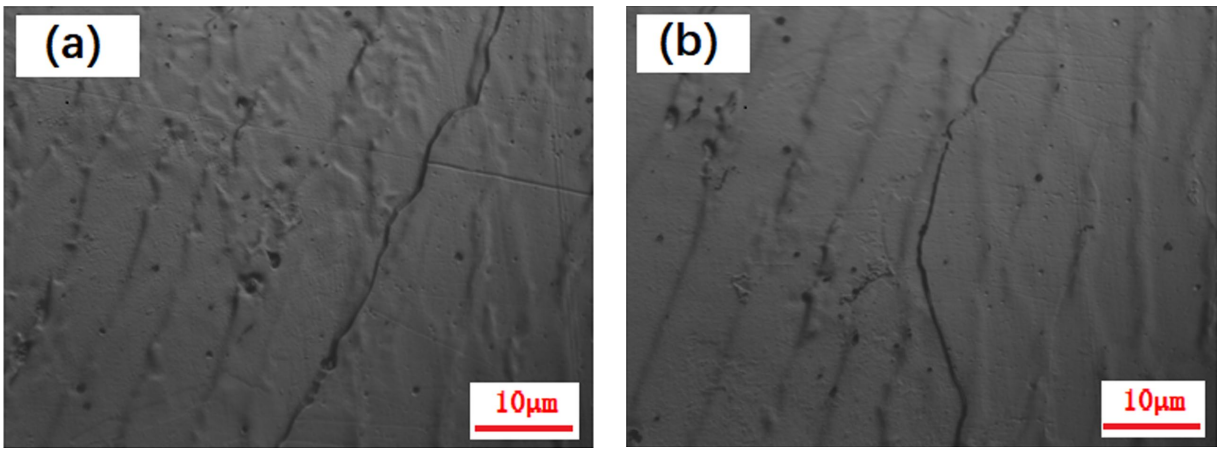

Fig. 10. Optical micrographs showing the solidification cracking during wire and laser additive manufacturing

morphology and solute concentration were carried out during transient conditions. The following conclusions can be drawn:

(1) A cluster of columnar dendrites are mainly distributed at the bottom of the cladding layers, one typical columnar dendrites are nearly vertical to the surface of substrate, the other typical columnar dendrites have a deflection angle to the normal direction of substrate surface. The columnar dendrites were almost distributed at the bottom of the substrate and then they grow along their preferred crystalline orientations in the shape of columnar dendrites during the wire and laser additive manufacturing (WLAM).

(2) At the early stage, the tip velocity of dendrite growth with interface crystallographic deflection is faster than that without interface crystallographic deflection. It can be

seen that the dendrite growth morphologies transform from symmetrical columnar dendrite to tilted columnar dendrite as the interface crystallographic deflection increasing.

(3) Increasing the deflection angle can lead to uneven composition of material matrix, especially at the columnar dendrite interface. The EDX results indicates that crystallographic orientation can increase the fluctuation of Cr element content. The predicted Cr concentration from the PF simulations agrees well with the EDX results of experiment. Solute concentrations at the columnar dendrite interface tend to promote hot cracking in additively manufactured Ni-based superalloy.

Acknowledgments

The present work is financially supported by The National Key Research and Development Program of China No. 2017YFB1103700.

REFERENCES

[1] Y.Y. Shi, C. Zhao, M. Qi, Y.B. Liu, P.F. Deng, Research on the cutting force of nickel based superalloy, Intelligent Systems Design and Engineering Applications **4**, 527-530 (2013).

[2] N. Zong, Y. Liu, S. Ma, W. Sun, T. Jing, H. Zhang, A review of chamfer technology in continuous casting process, Metallurgical Research & Technology **117**, 204-219 (2020).

[3] N. Zong, H. Zhang, Y. Liu, Z. Lu, Analysis of the off-corner subsurface cracks of continuous casting blooms under the influence of soft reduction and controllable approaches by a chamfer technology, Metallurgical Research & Technology **116**, 310-322 (2019).

[4] N. Zong, H. Zhang, Y. Liu, Z. Lu, Analysis on morphology and stress concentration in continuous casting bloom to learn the formation and propagation of internal cracks induced by soft reduction technology, Ironmaking and Steelmaking **46**, 872-885 (2019).

[5] N. Zong, Y. Liu, H. Zhang, X. Yang, Application of a chamfered slab technology to reduce straight edge seam defects of non-oriented silicon electrical steel generated during flexible thin slab casting process, Metallurgical Research & Technology **114**, 311-319 (2017).

[6] A. Cwudziński, Numerical and physical simulation of liquid steel behaviour in one strand tundish with subflux turbulence controller, Archives of Metallurgy and Materials **60**, 3, 1581-1586 (2015).

[7] A. Cwudziński, Numerical and physical modeling of liquid steel behaviour in one strand tundish with gas permeable barrier, Archives of Metallurgy and Materials **63**, 2, 589-596 (2018).

[8] T. Merder, Modelling the influence of changing constructive parameters of multi-strand tundish on steel flow and heat transfer, Ironmaking and Steelmaking **40**, 10, 1743-2812 (2016).

[9] T. Merder, Numerical analysis of the structure of liquid flow in the tundish with physical model verifocation, Archives of Metallurgy and Materials **63**, 4, 1895-1901 (2018).

[10] D. Ma, A.D. Stoica, Z. Wang, A.M. Beese, Crystallographic texture in an additively manufactured nickel-base superalloy, Materials Science and Engineering A **684**, 47-53 (2017).

[11] A. Woźniak, M. Adamiak, G. Chladek, J. Kasperski, The influence of the process parameters on the microstructure anf properties SLM processed 316L stainless steel, Archives of Metallurgy and Materials **65**, 1, 73-80 (2020).

[12] T. Pinomaaa, M. Lindroos, M.Walbrühl, N. Provatas, A. Laukkanen, The significance of spatial length scales and solute segregation in strengthening rapid solidification microstructures of 316L stainless steel, Acta Materialia **184**, 1, 1-16 (2020).

[13] Z. Dong, W. Zheng, Y. Wei, K. Song, Dynamic evolution of initial instability during non-steady-state growth, Physical Review E **89**, 062403 (2014).

[14] Z. Wang, S. Ma, W. Sun, M. Zhang, T. Jing, H. Dong, Cellular tip splitting instability during transient growth, Computational Materials Science **155**, 364-372 (2018).

[15] Z. Wang, T. Jing, H. Dong. Phase field study of spacing evolution during wire and laser additive manufacturing under transient conditions, IOP Conf. Series: Materials Science and Engineering **529**, 012003 (2019).

[16] W. Zheng, Z. Dong, Y. Wei, K. Song, Onset of the initial instability during the solidification of welding pool of aluminum alloy under transient conditions, Journal of Crystal Growth **402**, 203-209 (2014).